Journal of Cardiothoracic Surgery

RESEARCH Open Access

Characterization of prognostic signature related with twelve types of programmed cell death in lung squamous cell carcinoma

Saiyu Li[1], Bing Ding[1] and Duanli Weng[1*]

Abstract

Objective This study aimed to develop a prognostic cell death index (CDI) based on the expression of genes related with various types of programmed cell death (PCD), and to assess its clinical relevance in lung squamous cell carcinoma (LUSC).

Methods PCD-related genes were gathered and analyzed in silico using the transcriptomic data from the LUSC cohorts of The Cancer Genome Atlas (TCGA) and Clinical Proteomic Tumor Analysis Consortium (CPTAC). Differentially expressed PCD genes were analyzed, and a prognostic model was subsequently constructed. CDI scores were calculated for each patient, and their correlations with clinical features, survival outcomes, tumor mutation burden, gene clusters, and tumor microenvironment were investigated. Unsupervised consensus clustering was performed based on CDI model genes. Furthermore, the correlation of CDI for sensitivity of targeted drugs, chemotherapy efficacy, and immunotherapy responses was assessed.

Results Based on 351 differentially expressed PCD genes in LUSC, a CDI signature comprising FGA, GAB2, JUN, and CDKN2A was identified. High CDI scores were significantly associated with poor survival outcomes ($p < 0.05$). Unsupervised clustering revealed three distinct patient subsets with varying survival rates. CDKN2A exhibited significantly different mutation patterns between patients with high and low CDI scores ($p < 0.01$). High CDI scores were also linked to increased immune cell infiltration of specific subsets and altered expression of immune-related genes. Patients with high-CDI showed reduced sensitivity to several chemotherapeutic drugs and a higher Tumor Immune Dysfunction and Exclusion (TIDE) score, indicating potential resistance to immunotherapy.

Conclusion The CDI signature based on PCD genes offers valuable prognostic insights into LUSC, reflecting molecular heterogeneity, immune microenvironment associations, and potential therapeutic challenges. The CDI holds potential clinical utility in predicting treatment responses and guiding the selection of appropriate therapies for patients with LUSC. Future studies are warranted to further validate the prognostic value of CDI in combination with clinical factors and to explore its application across diverse patient cohorts.

Keywords Biomarker, Drug resistance, Immunotherapy resistance, Lung squamous cell carcinoma, Programmed cell death, Cell death index, Prognosis, Immunotherapy

*Correspondence:
Duanli Weng
DuanliWeng_FJMU@outlook.com

[1]Department of Respiratory and Critical Care Medicine, Longyan First Hospital, Affiliated to Fujian Medical University, 105 Jiuyi North Road, Longyan 364000, China

Introduction

Lung cancer is one of the most prevalent malignancies and a leading cause of cancer-related death worldwide [1, 2], yet its pathogenesis has not been fully clarified. Lung cancer is traditionally classified into two primary subtypes: small- (SCLC) and non-small-cell lung cancer (NSCLC), with the latter constituting approximately 85% of all cases. Only 24% of lung cancers are diagnosed at a localized stage, where the 5-year survival rate is 60%, while the overall 5-year survival rate for NSCLC is merely 26% [3]. The survival rate of lung cancer has been significantly improved in recent decades, with the pace accelerating attributing to remarkable advances in NSCLC treatment [4]. The treatment of NSCLC has evolved from the empirical use of cytotoxic regimens to the development of efficient and well-tolerated drugs targeting specific molecular subtypes [5]. However, the prognosis is still limited in some patients with NSCLC who are particularly resistant to chemotherapy or molecular targeting drugs [6]. The mechanism of drug resistance in NSCLC remains to be elucidated.

Programmed cell death (PCD) is a natural biological procedure and plays a vital role in both health and disease. PCD is essential for growth and development, as well as serving as a fundamental process for the rejuvenation of senescent cells. However, under certain circumstances, it can also facilitate pathological conditions. Thus, PCD is considered as a "double-edge sword," playing critical role in both organism homeostasis and pathogenesis. Recent evidence has revealed the significant effect of various types of PCD including apoptosis, necroptosis, ferroptosis, lysosome-dependent cell death, parthanatos, autophagy-dependent cell death, pyroptosis, netotic cell death, entotic cell death, oxeiptosis, and alkaliptosis [7–9]. For instance, necroptosis is a novel form of cell death that features morphological characteristics of necrosis as well as tight regulation [10]. Alkaliptosis is another type of PCD that is modulated by intracellular alkalinization [11]. While oxeiptosis utilizes the ROS sensing capabilities of KEAP1 to trigger a cell death process, which has recently been identified as a specific signaling pathway and is possibly to execute multiple PCD pathways together [12].

Programmed cell death (PCD) mechanisms play a crucial role in the pathogenesis of LUSC. Aberrations in these signaling pathways contribute to oncogenesis, tumor progression, and therapeutic resistance. In malignant cells, apoptotic mechanisms are often impaired, resulting in uncontrolled cellular proliferation and survival. The dysregulation of key apoptotic regulators such as p53, Bcl-2 family proteins, caspases, and inhibitors of apoptosis proteins (IAPs) is critically associated with lung cancer progression [13]. Research indicates that the abnormal expression of anti-apoptotic proteins such as Bcl-2 and Bcl-xL contributes to resistance against therapies designed to induce apoptosis in lung cancer [14]. Therapeutically targeting apoptosis pathways, using methods like BH3 mimetics or caspase activators, shows great potential in lung cancer treatment [15]. Necroptosis, another form of programmed cell death characterized by necrosis, is also gaining attention in lung cancer research. Though its role is less established compared to apoptosis and autophagy, emerging data suggest that necroptosis may play a part in lung cancer development, with a focus on crucial regulators like receptor-interacting protein kinase 3 (RIPK3). For instance, it was observed that low-level expression levels of the necroptosis markers RIPK3 and PELI1 are associated with an increased risk of mortality in patients with LUSC who underwent surgical tumor resection [16]. Autophagy plays a paradoxical role in lung cancer, functioning as both a tumor suppressor and a facilitator of tumor progression [17]. When autophagy is dysregulated, it supports lung cancer development by enhancing cell survival during stress and promoting tumor proliferation [18]. The relationship between autophagy and apoptosis in lung cancer cells is intricate, involving both cooperative and opposing interactions [19]. Targeting autophagic flux through pharmacological agents or genetic modification represents a promising strategy for lung cancer treatment. The autophagy-dependent cell death can be triggered by the interaction with RRM2 downregulation and further participates in the resistance to chemotherapeutic reagents such as gemcitabine in LUSC cells [20]. However, a comprehensive exploration of the association between multiple PCD patterns and LUSC remains elusive, and the specific roles of PCD in LUSC have been underexplored. Therefore, in the current study, we conducted array-based analysis to identify genes associated with survival for prognostic prediction aimed at guiding tailored treatments. In addition, this research may assist in determining appropriate therapeutic regimens for LUSC.

Methods

Study design

We compiled the PCD related genes from previous literature [21]. The PCD gene were then utilized for in silico analysis. The genomic expression patterns of LUSC versus normal lung tissue in The Cancer Genome Atlas (TCGA) database was explored, and differentially expressed genes (DEGs) were identified. The LUSC cohort in TCGA database was used for prognostic model construction via Lasso regression. The prognostic PCD signature was identified and a cell death index (CDI) calculation index was obtained. The transcriptomic data from the LUSC cohort in the Clinical Proteomic Tumor Analysis Consortium (CPTAC) database was then used

for external validation. The CDI score for each TCGA-LUSC patient was calculated. The correlations of CDI with clinical feature, survival outcomes, tumor mutation burden, gene cluster, tumor microenvironment and drug sensitivity were further explored.

Data processing and identification of DEGs between LUSC and normal lung tissue

The gene expression profiling data and clinical features of patients with LUSC in TCGA database were accessed via the Genomic Data Commons (GDC) data portal (https://portal.gdc.cancer.gov). The transcriptome profiling data from the TCGA-LUSC cohort were processed and normalized with the "DESeq2" package in R software. We further performed differentiation analysis for the expression of tested genes between the normal and LUSC samples by "DESeq2" package in R software. The PCD genes with |log2(fold change (FC))| > 1.0 and adjusted p value < 0.05 were considered as DEGs. The heatmap and volcano plots were generated to visualize these differentially expressed PCD genes by using the "ggplot2" package and "pheatmap" package in R software, respectively. Single-cell RNA sequencing data was obtained from GSE200972, which includes tumor RNA single-cell sequencing data for lung squamous cell carcinoma (LUSC). The single-cell sequencing data was processed using the Seurat package in R, and cell cluster annotation was performed using SingleR. Gene expression within different cell clusters was explored and compared.

Gene function enrichment analysis

Database for Annotation, Visualization and Integrated Discovery (DAVID, https://david.ncifcrf.gov/), an online tool that provided a comprehensive set of functional annotation was used to elucidate the biological significance of the identified DEGs. The enriched biological themes, particularly gene ontology (GO) terms as well as Kyoto Encyclopedia of Genes and Genomes (KEGG) pathway was analysed and further visualized by using the "ggplot2" package in R software.

Identification of prognostic PCD signature in LUSC

Univariate COX regression analysis was conducted in the TCGA-LUSC cohort to identify the PCD genes that were significant associated with survival in LUSC ($P<0.05$). Then, LASSO penalty analysis was conducted to shrink the overfitting by using "glmnet" package in R software. For the LASSO regression, we used a random seed of 123 and performed 10-fold cross-validation. Since our study focuses on time-to-event outcomes, we set the model parameter family to "cox". After cross-validation, we selected the λ value of "lambda.min", and the variables with coefficients that were not shrunk to zero were used for subsequent COX modeling. Finally, to obtain a novel prognostic PCD signature, a multivariate COX regression was analyzed via a stepwise process utilizing the "step" function from the "rms" package in R software. We set the parameter "direction" to "both", and the final model was obtained based on stepwise selection using the Akaike Information Criterion. The hazard ratio (HR) for each PCD signature model gene was illustrated in a forest plot by using the "survminer" package in R software. The CDI for each LUSC patient was calculated according to the expression level of PCD model genes using the following formula: CDI score = coefficient × (PCD gene-1 level) + coefficient × (PCD gene-2 level) + …… + coefficient × (PCD gene-n level).

Gene set variation analysis (GSVA) analysis in high- and low-CDI patients

The patients TCGA-LUSC cohort were divided into high- and low-CDI groups according to the median CDI score of the entire cohort. Differences in biological functions of the two groups were evaluated by GSVA method through the "c2.cp.reactome.v7.4.symbols.gmt" database, and "GSVA" and "GSEABase" packages in R software. The ridge plot was generated using the "ggplot2" and "ggridges" packages in R software.

Assessment of the prognostic performance of CDI

The relationship of survival status of TCGA-LUSC patients with CDI was evaluated by comparing the Kaplan-Meier curves between high- and low-CDI groups using the "survminer" package in R. ROC (receiver operating characteristic) curves and calibration curves at 1-, 3- and 5-year were generated to assess the accuracy of the CDI-predicted survival by using "pROC", "timeROC" and "rms" packages in R. The predictive performance of CDI was further validated using the transcriptomic data from the CPTAC -LUSC cohort employing the same methodologies.

Unsupervised consensus clustering

Based on the expression level of CDI model genes, consensus clustering analysis was conducted to identify distinct subsets of LUSC by using the "ConsensusClusterPlus" package in R. The distribution of survival status and CDI in the calculated PCD clusters were visualized by the "ggalluvial" and "ggplot2" packages in R software.

PCD genes mutation associated with CDI

The tumor mutation burden (TMB) data of the TCGA-LUSC cohort were obtained through the GDC data portal. The tumor mutation data was processed with "maftools" package in R. The most significantly differentially mutated PCD genes were identified and presented in a forest plot using the "forestPlot" function in "maftools" package in R. The mutation status of the PCD

model genes was further assessed by using the "coOncoplot" function in "maftools" package in R. Besides, more detailed information of the PCD model genes such as the location of the mutation on the gene segment was shown via lollipop plot using the "lollipopPlot2" function in "maftools" package in R.

The immune microenvironment in LUSC correlated with CDI

The immune related gene set, immune checkpoint gene set, HLA gene set were sourced from previous publication [22]. The prediction of immune infiltration in the LUSC tumor microenvironment was conducted using the CIBERSORT tool (https://cibersortx.stanford.edu/). There were a total of 22 types of immune infiltration cells analysed, including DC cells, M0/M1/M2 macrophages, T cells, B cells, etc. The correlation between these immune cells with CDI score was also examined.

Prediction of targeted drugs, chemotherapy sensitivity, and immunotherapy response correlated with CDI score

The sensitivity of targeted drugs and chemotherapeutic drugs was predicted based on the gene expression profile of each LUSC patient using the "oncoPredict" package in R. Inhibitory concentration (IC50) values of these drugs were calculated. The response to immunotherapy was estimated through the Tumor Immune Dysfunction and Exclusion (TIDE, https://tide.dfci.harvard.edu) method. The correlation of CDI score with the TIDE score, Dysfunction score and Exclusion score was analysed.

Statistical analysis

The statistical analysis in this research was conducted using R (version 4.2.2). The distribution normality for continuous variables was evaluated by Shapiro-Wilk test. If the continuous variables were normally distributed, they were compared by student's t-test; otherwise Wilcoxon ranked-sum test was conducted. In the differential expression analysis, we accounted for multiple testing by applying the Benjamini-Hochberg procedure to adjust the p-values. This method controls the false discovery rate (FDR), thereby reducing the likelihood of false positives. The adjusted p-values (q-values) were used to identify significantly differentially expressed genes (DEGs). P value <0.05 (two sides) was considered as statistically significant for all analysis.

Results

Identification of differentially expressed PCD genes in LUSC

The expression of PCD genes were compared between TCGA-LUSC tumor tissues and normal controls. Of these PCD genes, a total of 351 DEGs were identified, among which 176 were up-regulated and 175 were down-regulated (Fig. 1A and B). GO and KEGG revealed that the function of these DEGs were mainly enriched in regulating the apoptotic process, NF-kappa B signaling, ERK1/2 signaling, identical protein binding, lysosome, ferroptosis and pathways in cancer (Fig. 1C). These had indicated significant variations in the PCD genes expression profiles as well as their related biological functions in LUSC.

The STRING tool was employed to analyze the protein-protein interactions of the DEGs identified in our study. The analysis revealed significant clusters, with the four model genes (FGA, GAB2, JUN, and CDKN2A) as indicated in the next results section prominently situated within these clusters, underscoring their central roles in the network (Supplementary Figure S1A). Further validation was performed using Metascape and GeneMANIA. Metascape results highlighted key signaling pathways, including those related to apoptosis, autophagy, and ferroptosis, concentrated within the PPI networks (Supplementary Figure S1B). MCODE analysis of the PPI network identified nine critical clusters, with the four model genes acting as pivotal nodes (Supplementary Figure S1C). GeneMANIA analysis yielded similar conclusions, reinforcing the significance of our findings (Supplementary Figure S1D).

Development of the CDI score based on PCD model genes in predicting the prognosis of LUSC

The association between the DEGs and survival was evaluated by univariate COX regression, and 34 prognostic PCD genes were found to be significant ($p<0.05$). Next, Lasso-penalized regression was performed to eliminate the potential collinearity effect (Fig. 2A and B). Afterwards, eight PCD genes were preserved and included in the multivariate COX analysis (FGA, FES, GAB2, CHEK2, GGCT, JUN, CTSV and CDKN2A). Finally, with a stepwise selection process, four PCD genes were identified as model genes, namely FGA, GAB2, JUN and CDKN2A. The HRs, 95% confidence intervals (CI) and P values of these four included PCD genes in the final multivariate COX model were shown in Fig. 2C. The constructed PCD signature was presented as a PCD model gene-expression level calculated CDI score using the following formula: CDI score $=0.0779 * FGA + 0.1619 * GAB2 + 0.1859 * JUN - 0.0504 * CDKN2A$. LUSC patients that died during follow-up showed a significantly higher CDI score (Fig. 2D). The correlation of CDI with various clinical features such as gender, age and tumor stage were also depicted in Fig. 2D.

We further investigated the distribution of the four model genes in five cell types detected by single-cell sequencing in LUSC (Supplementary Figure s2). FGA showed relatively low overall expression, primarily localized in epithelial cells. GAB2 was highly expressed not

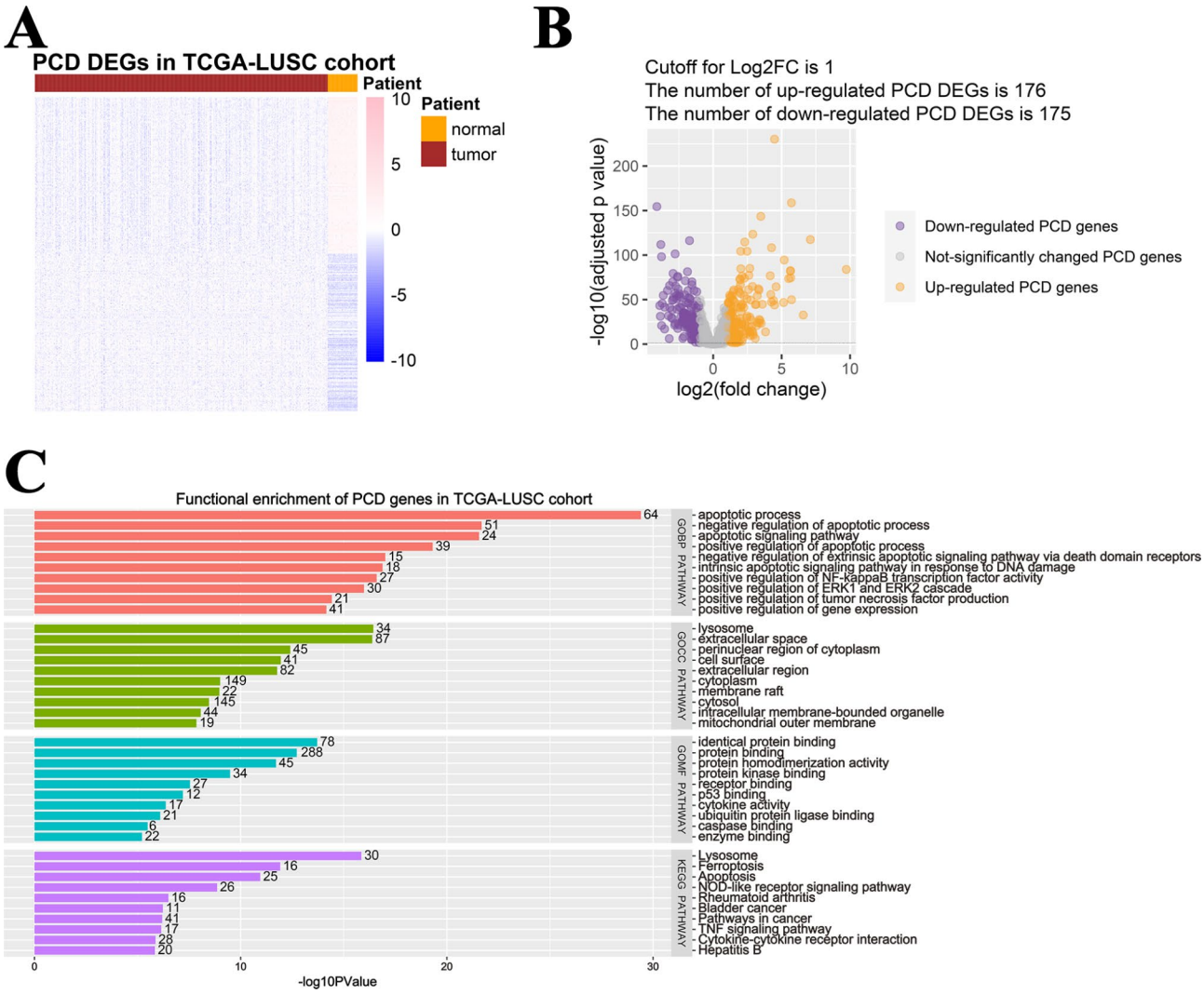

Fig. 1 Differential Expression of PCD Genes in LUSC. (**A**) Heatmap illustrating the differential expression of PCD genes in TCGA-LUSC tumor tissues compared to normal controls. A total of 351 differentially expressed genes (DEGs) were identified, with 176 up-regulated (red) and 175 down-regulated (blue). (**B**) Volcano plot representing the fold change (log2) on the x-axis and the adjusted p-value (– log10) on the y-axis for the DEGs. The threshold for significance was set at |log2(fold change)| > 1.0 and adjusted p-value < 0.05. (**C**) Functional enrichment analysis of DEGs showing enriched biological themes, including gene ontology (GO) terms and Kyoto Encyclopedia of Genes and Genomes (KEGG) pathways. These DEGs were primarily associated with regulating the apoptotic process, NF-kappa B signaling, ERK1/2 signaling, identical protein binding, lysosome, ferroptosis, and pathways in cancer. PCD - Programmed Cell Death; LUSC - Lung Squamous Cell Carcinoma; TCGA - The Cancer Genome Atlas

only in epithelial cells but also in NK cells. JUN exhibited a high positive expression rate across the cell population, predominantly in T cells and NK cells, whereas CDKN2A was mainly expressed in another cluster of epithelial cells. The CDI for each single cell, calculated based on the expression levels of these four genes, was highest in NK cells, followed by T cells.

To further understand the biological status changes that are potentially related with CDI, GSVA analysis was performed to compare high- and low-CDI patients. High CDI and low CDI groups were defined based on the median CDI value calculated from the entire patient cohort. Patients with CDI values above the median were categorized into the high CDI group, while those below or equal to the median were categorized into the low CDI group. It was found that LUSC patients with higher CDI might be associated with activated pathways such as complement and coagulation cascades, PPAR signaling, primary bile acid metabolism, etc. (Figure 2E and F). These have identified a prognostic signature composed of four key PCD genes (FGA, GAB2, JUN, CDKN2A) whose expression levels correlate with survival in LUSC, and further analysis suggests that higher CDI scores are associated with activation of pathways involved in coagulation, lipid metabolism, and immune response.

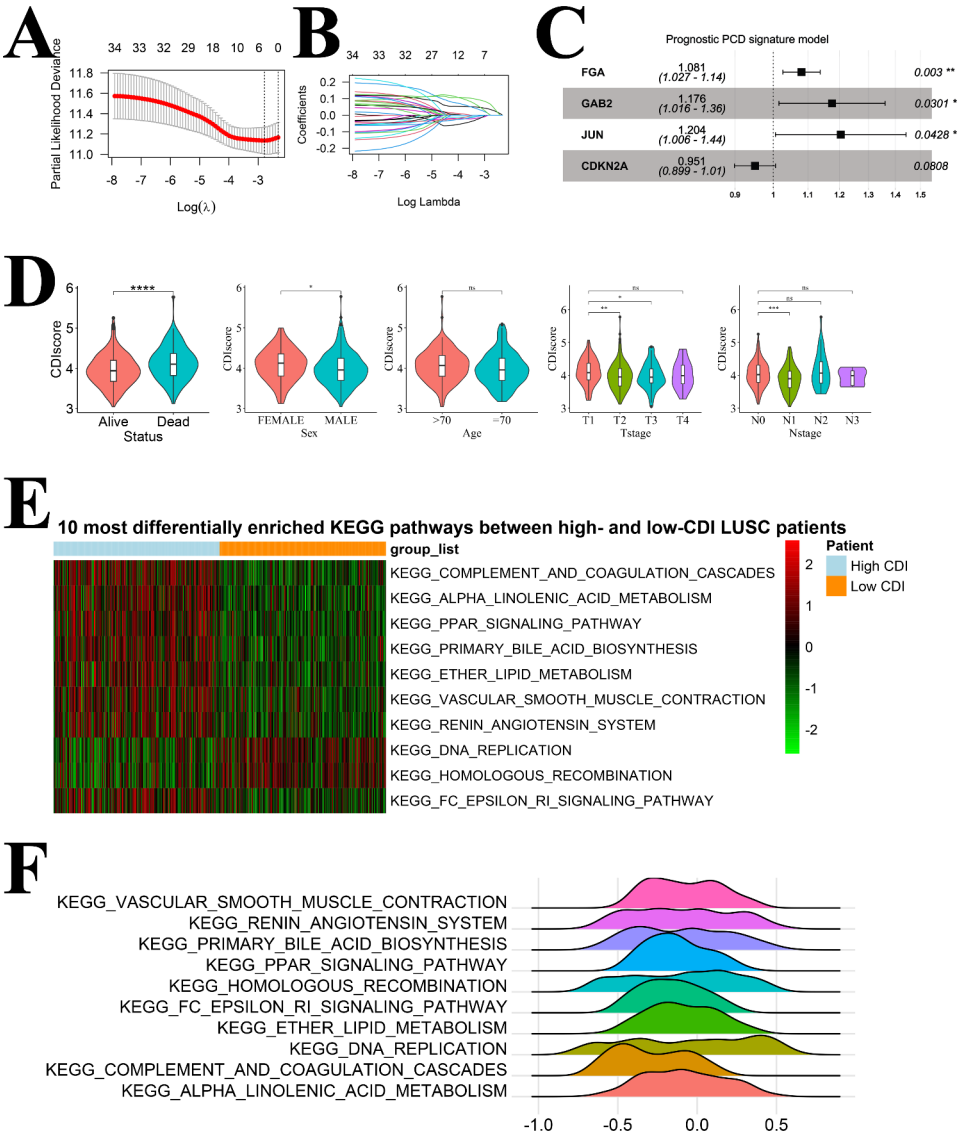

Fig. 2 Development of the CDI Score and Prognostic PCD Signature in LUSC. (**A**) and (**B**) Lasso penalty analysis was performed to select PCD genes and eliminate potential overfitting. (**C**) Forest plot illustrating the hazard ratios (HRs), 95% confidence intervals (CI), and p-values for the four selected PCD model genes (FGA, GAB2, JUN, and CDKN2A) in the final multivariate COX model. (**D**) Comparison of CDI scores between LUSC patients who died during follow-up and those who survived. (**E**) Gene Set Variation Analysis (GSVA) showing differences in biological functions between high-CDI and low-CDI patients. High-CDI patients exhibited activation of pathways such as complement and coagulation cascades and PPAR signaling. PCD - Programmed Cell Death; CDI - Cell Death Index; LUSC - Lung Squamous Cell Carcinoma; TCGA - The Cancer Genome Atlas

Validation of the prognostic value of the CDI in LUSC patients

Kaplan-Meier curves of the high- and low-CDI patient groups exhibited a distinct dispersed pattern in both the TCGA and CPTAC cohorts with P value < 0.05 (Fig. 3A), and higher CDI was associated with a significantly worse survival outcome (Fig. 3B). The distribution of expression levels of each PCD model gene across different survival outcome groups was also consistent with their HRs (Fig. 2C and B). At 1-, 3- and 5-year of follow up timepoint, the CDI prediction obtained AUROC values of almost all >0.8 (Fig. 3C), indicating robust predictive performance. In the TCGA-LUSC cohort, the 1-, 3-, and 5-year predictions align well with the actual outcomes (Fig. 3D), demonstrating the performance of the CDI in predicting survival probabilities. However, in the CPTAC-LUSC cohort, the CDI slightly underestimates the 1-year and 3-year survival probabilities for patients with an actual prognosis close to 100%, predicting around 95–97% (Fig. 3E). Despite this, the predictions remain close to the actual outcomes. Additionally, all other point estimates have 95% confidence intervals (CIs) that cross the reference line, indicating a satisfactory fit overall. These findings highlight the efficacy of the CDI

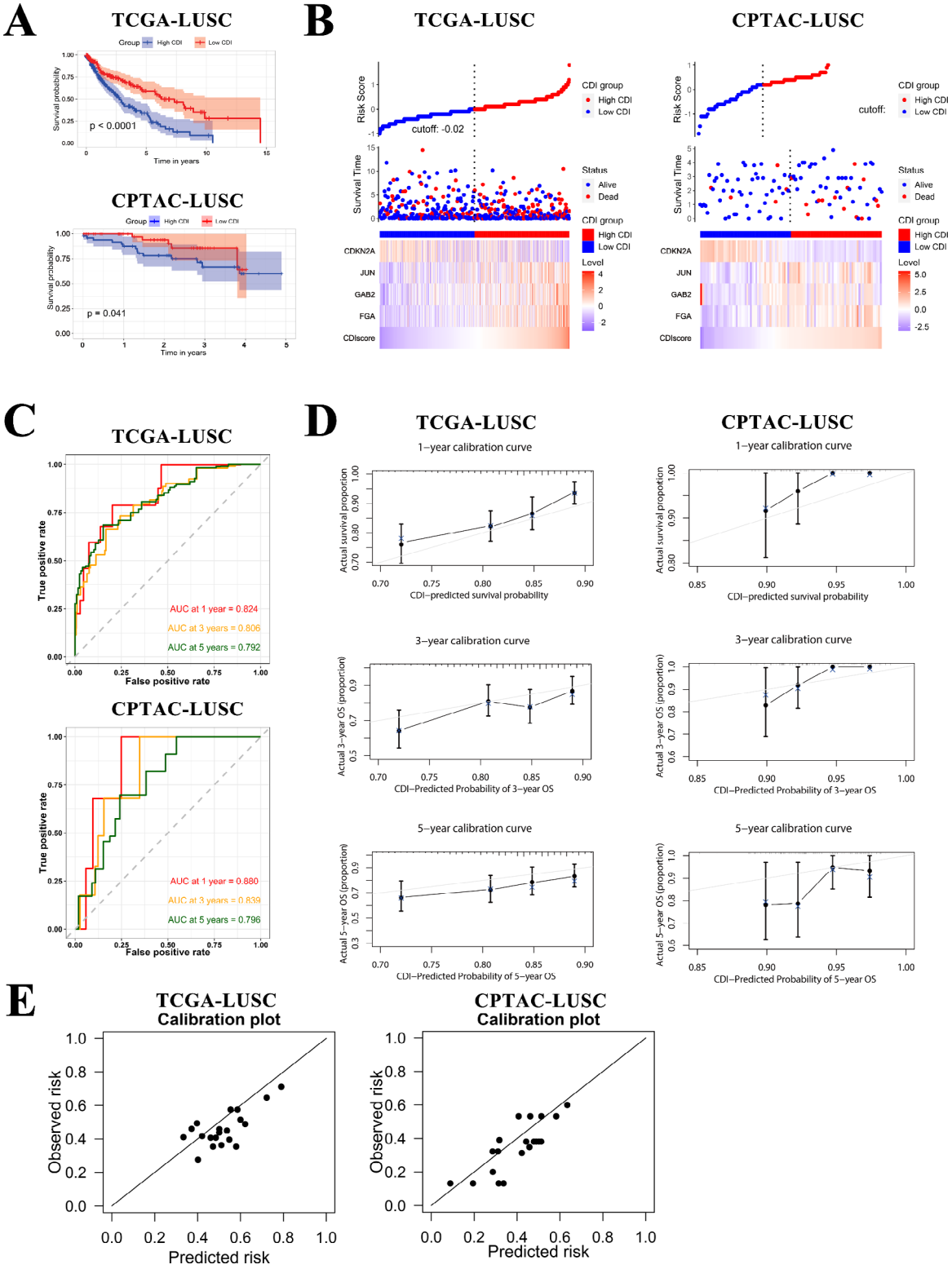

Fig. 3 Validation of the Prognostic Value of the CDI Score in LUSC Patients. (**A**) Kaplan-Meier survival curves comparing high- and low-CDI patient groups in both the TCGA and CPTAC cohorts. (**B**) Higher CDI scores were associated with significantly worse survival outcomes. (**C**) Receiver operating characteristic (ROC) curves at 1-, 3-, and 5-year follow-up timepoints, demonstrating the predictive performance of CDI. (**D**) and (**E**) Calibration curves comparing the predicted CDI outcomes with the observed results in the TCGA cohort. CDI - Cell Death Index; LUSC - Lung Squamous Cell Carcinoma; TCGA - The Cancer Genome Atlas; CPTAC - Clinical Proteomic Tumor Analysis Consortium

in providing reliable survival predictions, although slight discrepancies in high-prognosis patients warrant further investigation.

Unsupervised consensus clustering by PCD model genes

The four PCD model genes were utilized to conduct consensus clustering among TCGA-LUSC patients to delineate distinct subtypes. As shown in Fig. 4A and B, we chose 3 as the k value since the relative change in area under CDF curve reduced to a remarkable low level when k>3. Therefore, LUSC patients can be classified into three subsets which presented as different consensus clusters (Fig. 4C). It was observed that these three subsets of LUSC patients had significantly varied results of survival rates (Fig. 4D). Cluster 2 had a notably higher proportion of patients with low CDI as well as a higher proportion of surviving patients (Fig. 4E). In brief, the consensus clustering of TCGA-LUSC patients based on the 4 PCD model genes revealed three distinct subtypes, each associated with varied survival rates and CDI levels, suggesting potential prognostic implications.

PCD genes mutation in high- and low-CDI patients

The mutation of PCD genes were assessed patients stratified by high- and low-CDI levels. Figure 5A delineated the most distinct mutation of PCD genes between two groups with P of difference<0.01. Among the four PCD model genes, only CDKN2A exhibited significant variation in mutation status between patients with high- and low-CDI levels with $P<0.01$. We further investigated the four PCD model genes in terms of specific types of gene mutation. As shown in Fig. 5B, GAB2 and JUN showed minor missense mutation in low-CDI patients. FGA had minor nonsense mutation in high-CDI group. Conversely, CDKN2A had very significantly varied types of mutation between CDI groups, with low-CDI group had more quantity of mutations. More details of these mutations are shown in Fig. 5C. The differential mutation patterns of PCD genes, particularly CDKN2A, suggest potential prognostic implications in LUSC based on CDI stratification.

CDI score associated with different immune status

Figure 6A illustrates the top 20 immune related genes, immune checkpoint genes and HLA genes that were

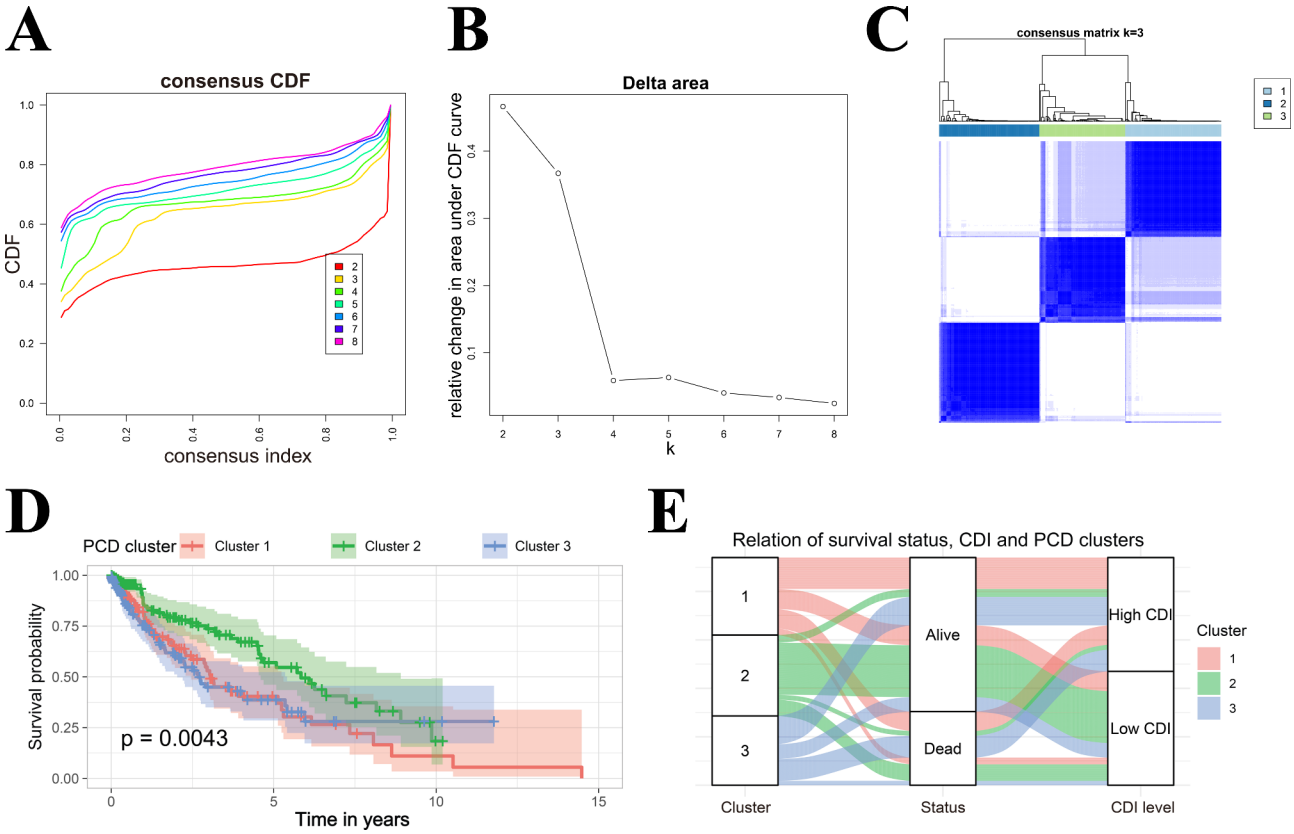

Fig. 4 Unsupervised Consensus Clustering by PCD Model Genes. (**A**) and (**B**) Selection of the optimal number of clusters (k) based on the relative change in the area under the cumulative distribution function (CDF) curve. (**C**) Consensus clustering analysis using the four PCD model genes identified three distinct subsets of LUSC patients. (**D**) Survival rate differences among the three subsets of LUSC patients. (**E**) Proportion of low-CDI patients and survivors in each cluster. PCD - Programmed Cell Death; CDI - Cell Death Index; LUSC - Lung Squamous Cell Carcinoma

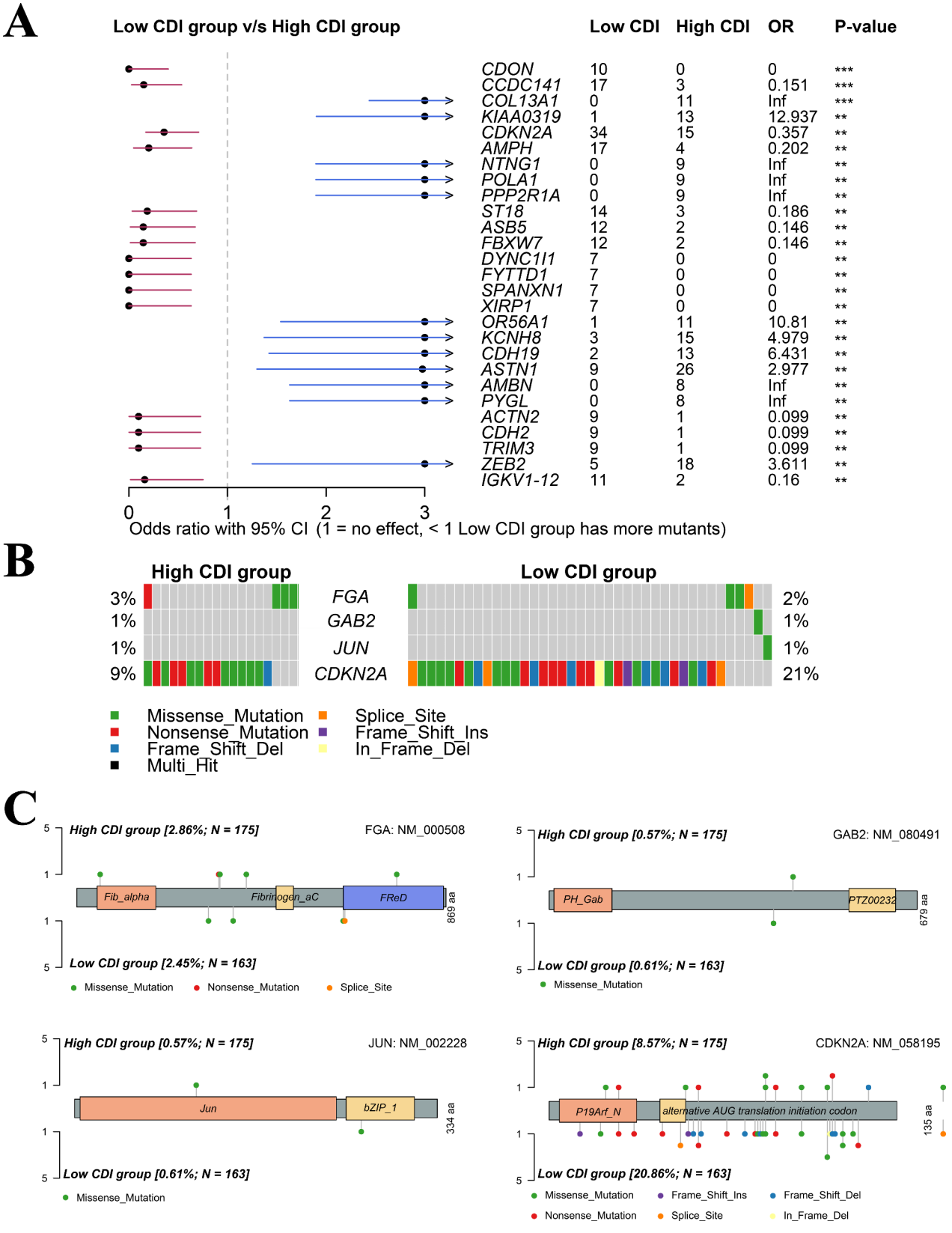

Fig. 5 PCD Genes Mutation in High- and Low-CDI Patients. (**A**) Forest plot illustrating the most significantly differentially mutated PCD genes between high- and low-CDI patients. (**B**) Specific types of gene mutations in the four PCD model genes (FGA, GAB2, JUN, and CDKN2A) in relation to CDI groups. (**C**) Lollipop plot showing the location of mutations on the gene segments of CDKN2A in high-CDI and low-CDI groups. PCD - Programmed Cell Death; CDI - Cell Death Index

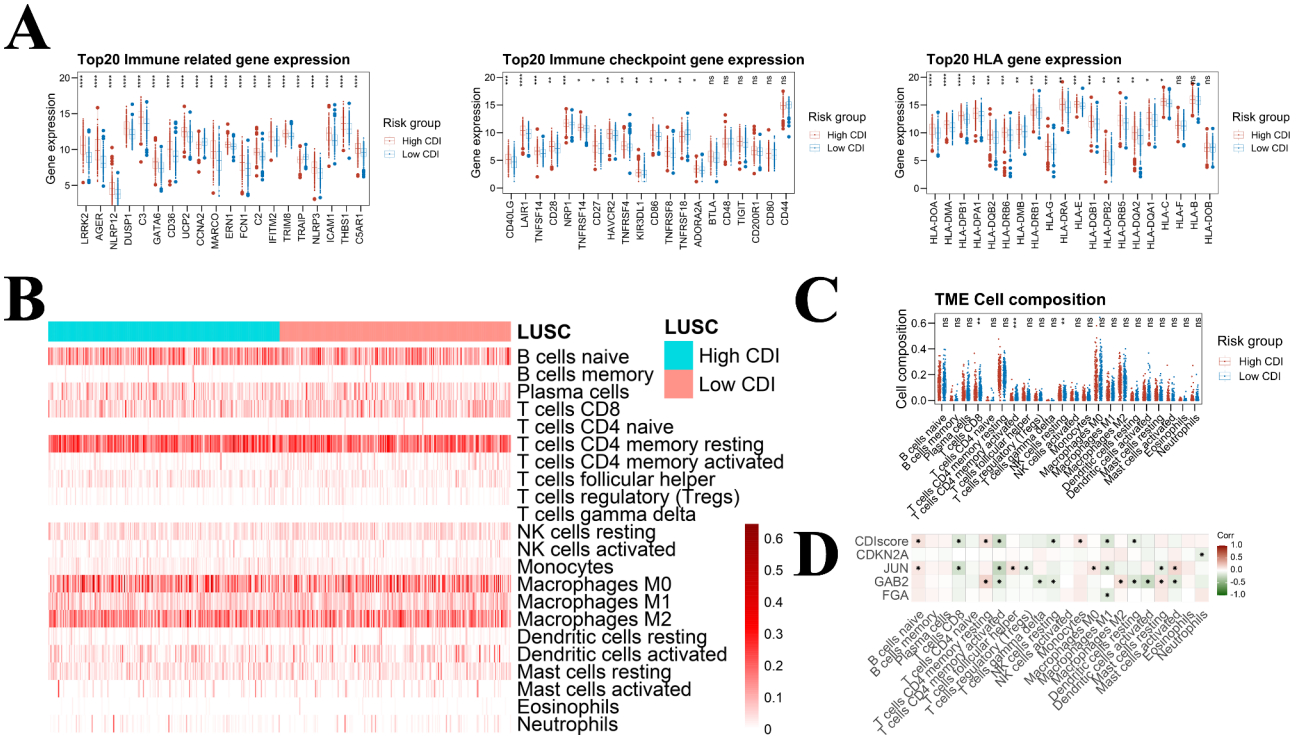

Fig. 6 CDI Score Associated with Different Immune Status. (**A**) Top 20 differentially expressed immune-related genes, immune checkpoint genes, and HLA genes between high- and low-CDI groups. **B**) Proportion of immune infiltration for 22 types of immune cells in high- and low-CDI groups. (**C**) Significantly altered immune cell subsets between high- and low-CDI groups. (**D**) Correlation between CDI score and immune cell infiltration. CDI - Cell Death Index; HLA - Human Leukocyte Antigen

most differently expressed in high- and low-CDI groups. The substantial alterations in the expression of immune-related genes underscore marked variations in immune status. Subsequently, the proportion of immune infiltration was evaluated for 22 types of immune cells (Fig. 6B). In total, CD8+T cells, activated CD4+T memory cells and resting NK cells were significantly changed between high- and low-CDI groups (Fig. 6C). When handled as a continuous variable, CDI score was significantly positively related with the infiltration of naive B cells, resting CD4+T memory cells, monocytes, and negatively related with the infiltration of CD8+T cells, activated CD4+T memory cells, resting NK cells, M1 macrophages and resting dendritic cells (Fig. 6D). These findings suggested that the differential expression of immune genes showed significant immune profile variations between CDI groups.

Estimate of response to chemotherapy, targeting drugs and immunotherapy based on CDI

Figure 7A depicted the top 10 drugs significantly associated with CDI-predicted response to. Notably, several EGFR-TKIs such as afatinib, erlotinib, gefitinib and osimertinib were included. Besides, among the four PCD model genes, the gene expression of FGA showed more significant relevance with these top 10 drugs, suggesting that gene FGA might contribute the most to drug resistance in LUSC. We also evaluated several commonly used chemotherapeutic drugs as shown in Fig. 7B. The IC50 values of cisplatin and gemcitabine were not different in high- and low-CDI groups; while paclitaxel, docetaxel and vinorelbine had significantly higher IC50 values in high-CDI group.

Regarding the prediction of immunotherapy, the high-CDI group exhibited a significantly elevated TIDE scores (Fig. 7C), suggesting a higher likelihood of tumor immune evasion and reduced potential benefit from immunotherapy. Furthermore, while the dysfunction scores were higher, the exclusion scores were lower in high-CDI group, implying that the immune evasion of LUSC tumor cells in high-CDI patients may be predominantly stem from T cell dysfunction. Overall, the high expression of FGA in LUSC correlates significantly with resistance to EGFR-TKIs, suggesting its pivotal role in drug resistance. Additionally, high CDI predicts reduced efficacy of paclitaxel, docetaxel, and vinorelbine, and indicates poorer immunotherapy outcomes due to increased TIDE scores and T cell dysfunction.

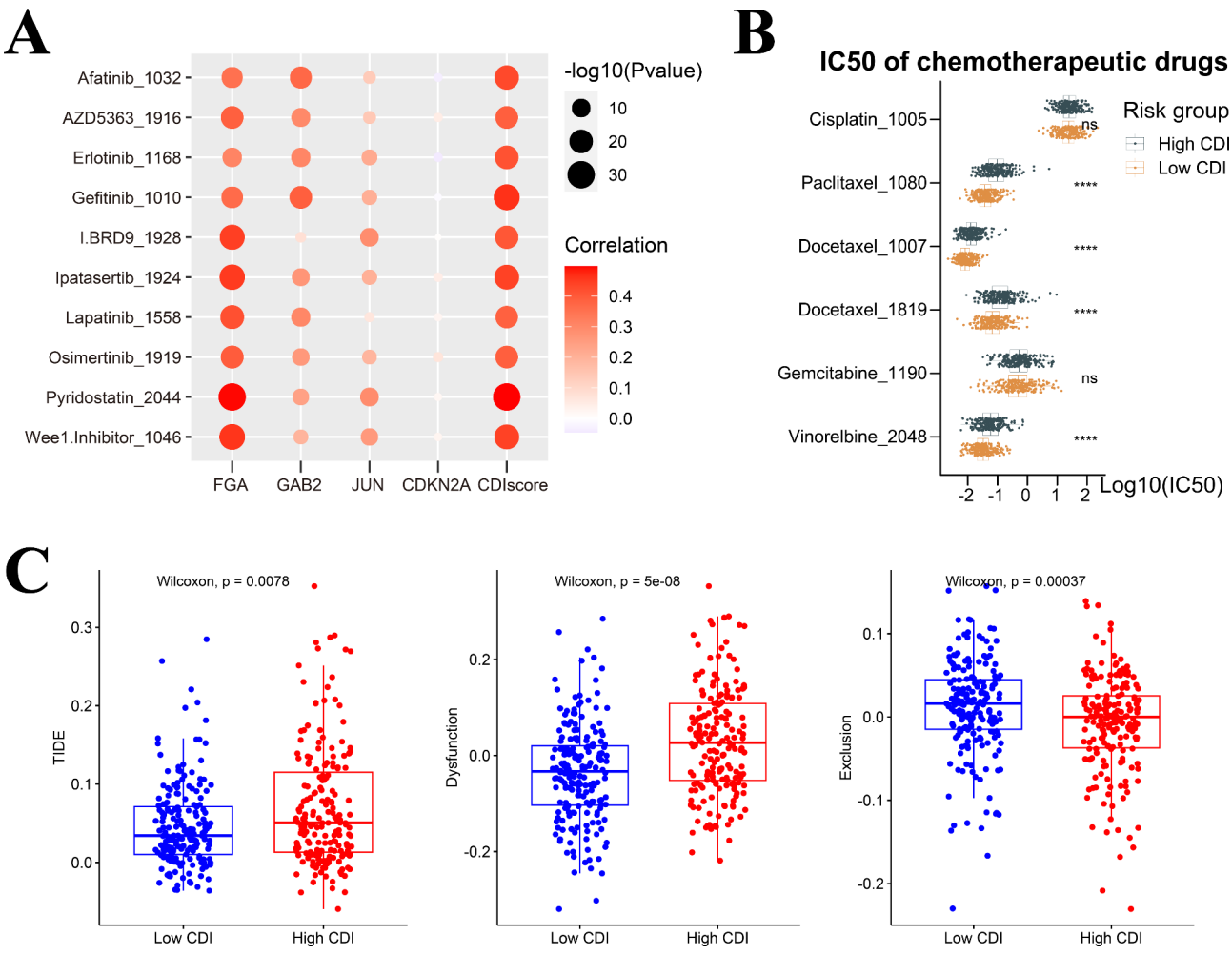

Fig. 7 Estimate of Response to Chemotherapy, Targeted Drugs, and Immunotherapy Based on CDI. (**A**) Top 10 drugs with predicted responses significantly related to CDI scores, including several EGFR-TKIs. (**B**) Evaluation of the sensitivity to commonly used chemotherapeutic drugs in high- and low-CDI groups. (**C**) TIDE score, Dysfunction score, and Exclusion score indicating the response to immunotherapy in high-CDI and low-CDI groups. CDI - Cell Death Index; EGFR-TKIs - Epidermal Growth Factor Receptor Tyrosine Kinase Inhibitors; TIDE - Tumor Immune Dysfunction and Exclusion

Discussion

This study has demonstrated a significantly altered gene expression pattern of twelve types of programmed cell death in LUSC, based on which a cell death index related with the prognosis was further developed. The CDI included four critical PCD genes which showed specific mutation patterns, and was correlated with several immunocytes that were related with tumor immune microenvironment. The constructed CDI shows significant associations with the sensitivity to multiple commonly used drugs such as chemotherapy and targeting drugs in LUSCpatients. The level of CDI also featured the potential to predict patient responses to immunotherapy. Our study underscores the pivotal role of PCD model genes in LUSC prognosis and highlights the CDI's promise in guiding the selection of appropriate therapies for sensitive patients.

A total of four PCD genes (FGA, GAB2, JUN and CDKN2A) were included in the prognostic model. These four genes are related with apoptosis (FGA and JUN), lysosome-dependent cell death (GAB2) and cuproptosis (CDKN2A). FGA, the gene encoding the alpha component of fibrinogen, plays a crucial role in blood clot formation following vascular injury [23]. In the context of LUSC, FGA has been implicated in tumor growth and metastasis. A recent study using CRISPR/Cas9 to knock out FGA in human lung cancer cell lines demonstrated increased cell proliferation, migration, and invasion, accompanied by a reduction in epithelial markers such as E-cadherin [24]. This knockout also promoted tumor growth and metastasis in vivo through the integrin-AKT signaling pathway, highlighting FGA's potential role in LUSC progression [24]. GAB2 is a member of the GRB2-associated binding protein family, known for its role in signal transduction through cytokine and growth

factor receptors. GAB2 has been identified as a key activator of the phosphatidylinositol-3 kinase (PI3K) pathway in response to various stimuli [25]. In LUSC, GAB2 has been linked to tumor progression through its regulation by non-coding RNAs, particularly SNORA38B. SNORA38B has been shown to enhance GAB2 expression, thereby activating the AKT/mTOR pathway, which promotes cell proliferation, migration, and invasion while inhibiting apoptosis [26]. Furthermore, SNORA38B-mediated GAB2 activation also contributes to an immunosuppressive tumor microenvironment, which can reduce the efficacy of immune checkpoint blockade therapies [26]. The JUN gene encodes a protein that interacts with specific DNA sequences to regulate gene expression, and it is a putative transforming gene of avian sarcoma virus 17 [27]. In LUSC, JUN plays a significant role in the tumor microenvironment, particularly in response to PD-1/PD-L1 blockade immunotherapy. JUN has been identified as a biomarker of response to PD-1 blockade therapy. Re-analysis of single-cell RNA sequencing data from lung adenocarcinoma patients undergoing PD-1 blockade revealed that JUN expression is associated with the presence of non-exhausted CD8+T cells, which are critical for effective anti-tumor immunity [28]. These findings suggest that JUN may influence the effectiveness of PD-1 blockade therapy in LUSC by modulating the tumor microenvironment. CDKN2A generates multiple transcript variants encoding proteins that function as inhibitors of CDK4 kinase, playing a crucial role in cell cycle regulation. Loss-of-function (LOF) mutations in CDKN2A have been associated with poor prognosis in LUSC. A study involving patients with advanced NSCLC who underwent next-generation sequencing prior to immune checkpoint blockade therapy found that CDKN2A LOF was linked to inferior progression-free survival and OS [29]. This negative impact was observed even in patients with high TMB and high PD-L1 expression, suggesting that CDKN2A LOF tumors are more likely to progress following immunotherapy [29]. These findings highlight the potential of CDKN2A as a therapeutic target and a prognostic marker in LUSC.

Lysosome-dependent cell death is characterized by the destabilization of lysosomal and has recently been recognized as a subtype of programmed cell death [30]. Given that many types of tumors, including LUSC, exhibit rapid cell proliferation and heightened cell survival processes in response to cellular injury, multiple transformation-related alterations at the level of the lysosome help to keep the cells against lysosome-dependent cell death. However, the contrary impact is also discovered, where cancer cells may exploit the stability of lysosome to enhance their carcinogenesis potential and invasiveness [31]. Therefore, it is crucial to investigate the intricate modulation of lysosomal membrane permeabilization in tumor cells for pharmacologically targeting lysosome-dependent cell death for therapeutic purposes. Our study reveals that GAB2 is an independent risk factor (HR=1.176, P=0.03) for the survival of LUSC patients. Additionally, GAB2 can be regulated by the small nucleolar RNA, SNORA38B, which is upregulated in NSCLC cells and correlates with a poor prognosis [26]. SNORA38B promotes GAB2 transcription, thereby activating protein kinase B (AKT)/mammalian target of rapamycin (mTOR) pathway through directly binding with E2F1, thus enhancing NSCLC progression. The SNORA38B/GAB2/AKT/mTOR pathway is also associated in the recruitment of CD4+FOXP3+regulatory T cells by stimulating the secretion of interleukin 10 by cancer cells, thus inhibiting the infiltration of CD3+CD8+T cells in the LUSC tumor microenvironment, and further facilitating cancer cells proliferation and worse immune efficacy. Consequently, the PCD genes identified in the current study represent novel markers and potential therapeutic targets, which should be validated in the future research of LUSC.

To further elucidate the clinical utility of the CDI, specific implementation steps could involve the integration of CDI assessment into routine clinical workflows for LUSC patients. Notably, the CDI is derived from the expression levels of only four genes, which makes it a potentially cost-effective tool for clinical application. Following initial diagnosis, the CDI could be calculated using gene expression profiling of biopsy samples. This molecular-level prognostic tool could be used alongside traditional clinical factors such as age, gender, and tumor stage to stratify patients into different risk categories. High CDI scores might indicate a higher likelihood of response to specific therapies such as chemotherapy, targeted therapy, or immunotherapy. Conversely, patients with low CDI scores could be considered for alternative therapeutic strategies or enrollment in clinical trials investigating novel treatments. The use of CDI is analogous to the COVID-19 critical illness prediction model developed during the pandemic [32]. Similar to how the COVID-19 risk score uses a few simple parameters multiplied by coefficients to predict the risk of critical illness, CDI uses gene expression data to estimate the future risk of specific outcomes, guiding clinical decisions and enabling personalized interventions. Future work should focus on conducting prospective clinical trials to validate the predictive accuracy of CDI in diverse patient cohorts and to develop standardized protocols for its clinical application. Moreover, case studies illustrating successful application of CDI-guided treatment decisions could provide valuable insights and further substantiate its clinical relevance.

There are several limitations of this study. The prognostic performance of the CDI constructed in the current

study has not yet been further evaluated by combining with clinical factors such as age, gender, tumor stage, etc. A nomogram containing CDI and certain critical clinical factors might be of help to predict patient survival. Our study cohort for LUSC is relatively small compared to other tumor types, which may limit the robustness of certain data analyses, such as in identifying differentially expressed genes (DEGs). The smaller sample size increases the risk that potentially significant genes may not reach statistical significance in our analysis. Additionally, our reliance on publicly available databases such as TCGA and CPTAC introduces inherent limitations including the potential for selection bias due to ambiguous patient selection criteria and geographical variability in genetic predispositions. Lastly, the lack of in vivo and in vitro experiments is a major limitation, and the impact of the core genes such as CDKN2A on the oncological phenotype of lung squamous carcinoma should be addressed in future research endeavors.

In conclusion, this study has showed a significantly altered gene expression pattern in PCD in LUSC, leading to the development of a prognostic CDI. The CDI, comprising four key PCD genes (FGA, GAB2, JUN, and CDKN2A), correlates strongly with LUSC prognosis, immune cell infiltration, and drug sensitivity to chemotherapy, targeted therapy, and immunotherapy. Notably, CDI has potential clinical utility in predicting treatment responses and aiding in the selection of appropriate therapies for LUSC patients. Future studies are needed to further validate the prognostic value of CDI in combination with clinical factors and explore its application in diverse patient cohorts.

Supplementary Information

The online version contains supplementary material available at https://doi.org/10.1186/s13019-024-03039-5.

Supplementary Material 1: Protein-Protein Interaction (PPI) Network and Functional Enrichment Analysis of Differentially Expressed Genes (DEGs). (A) STRING analysis of the DEGs identified in this study, revealing significant clusters within the PPI network. The four model genes (FGA, GAB2, JUN, and CDKN2A) are prominently situated within these clusters, underscoring their central roles in the network. (B) Metascape functional enrichment analysis of the PPI network. The results highlight key signaling pathways, including apoptosis, autophagy, and ferroptosis, concentrated within the PPI networks.(C) MCODE analysis of the PPI network, identifying nine critical clusters. The four model genes act as pivotal nodes within these clusters.(D) GeneMANIA analysis, which reinforces the significance of the findings and supports the central roles of the four model genes in the network

Supplementary Material 2: Expression Distribution of Model Genes in Single-Cell Sequencing Data from LUSC. (A) Spatial distribution of the expression of four model genes (FGA, GAB2, JUN, and CDKN2A) in five identified cell types (epithelial cells, NK cells, T cells, and others) within lung squamous cell carcinoma. (B) Bar charts illustrating the expression levels of the four model genes (FGA, GAB2, JUN, and CDKN2A) across different cell types

Acknowledgements
None.

Author contributions
DW: Conceived the study, designed the research, collected and assembled the data, participated in data analysis and interpretation, drafted the manuscript, and gave final approval of the manuscript. BD: Provided administrative support, participated in the conception and design of the study, reviewed and supervised the manuscript, and gave final approval of the manuscript. SL: Collected and assembled the data, participated in data analysis and interpretation, drafted the manuscript, and gave final approval of the manuscript. All authors read and approved the final manuscript.

Funding
None.

Data availability
No datasets were generated or analysed during the current study.

Declarations

Ethics approval and consent to participate
Not applicable.

Consent for publication
Not applicable.

Conflict of interest
The authors have no conflicts of interest to declare.

Received: 10 December 2023 / Accepted: 30 August 2024
Published online: 01 October 2024

References

1. Jenkins R, Walker J, Roy UB. 2022 cancer statistics: focus on lung cancer. Future Oncol. 2023.
2. Xiang D, Hu S, Mai T, Zhang X, Zhang L, Wang S, et al. Worldwide cancer statistics of adults over 75 years old in 2019: a systematic analysis of the global burden of disease study 2019. BMC Public Health. 2022;22(1):1979.
3. Heist RS, Sequist LV, Engelman JA. Genetic changes in squamous cell lung cancer: a review. J Thorac Oncology: Official Publication Int Association Study Lung Cancer. 2012;7(5):924–33.
4. Cheng Y, Zhang T, Xu Q. Therapeutic advances in non-small cell lung cancer: focus on clinical development of targeted therapy and immunotherapy. MedComm. 2021;2(4):692–729.
5. Sun Y, Yin X, Wen MM, Zhang J, Wang XJ, Xia JH, et al. EGFR mutations subset in Chinese lung squamous cell carcinoma patients. Mol Med Rep. 2018;17(6):7575–84.
6. Acker F, Stratmann J, Aspacher L, Nguyen NTT, Wagner S, Serve H, et al. KRAS mutations in squamous cell carcinomas of the lung. Front Oncol. 2021;11:788084.
7. Wang H, An P, Xie E, Wu Q, Fang X, Gao H, et al. Characterization of ferroptosis in murine models of hemochromatosis. Hepatology. 2017;66(2):449–65.
8. Shi J, Zhao Y, Wang K, Shi X, Wang Y, Huang H, et al. Cleavage of GSDMD by inflammatory caspases determines pyroptotic cell death. Nature. 2015;526(7575):660–5.
9. Fuchs Y, Steller H. Live to die another way: modes of programmed cell death and the signals emanating from dying cells. Nat Rev Mol Cell Biol. 2015;16(6):329–44.
10. Degterev A, Huang Z, Boyce M, Li Y, Jagtap P, Mizushima N, et al. Chemical inhibitor of nonapoptotic cell death with therapeutic potential for ischemic brain injury. Nat Chem Biol. 2005;1(2):112–9.
11. Song X, Zhu S, Xie Y, Liu J, Sun L, Zeng D, et al. JTC801 induces pH-dependent death specifically in Cancer cells and slows growth of tumors in mice. Gastroenterology. 2018;154(5):1480–93.
12. Scaturro P, Pichlmair A. Oxeiptosis: a discreet way to respond to radicals. Curr Opin Immunol. 2019;56:37–43.
13. Hanahan D, Weinberg RA. Hallmarks of cancer: the next generation. Cell. 2011;144(5):646–74.

14. Fennell DA. Caspase regulation in non-small cell lung cancer and its potential for therapeutic exploitation. Clin Cancer Res. 2005;11(6):2097–105.
15. Wong RS. Apoptosis in cancer: from pathogenesis to treatment. J Exp Clin Cancer Res. 2011;30(1):87.
16. Lim JH, Oh S, Kim L, Suh YJ, Ha YJ, Kim JS, et al. Low-level expression of necroptosis factors indicates a poor prognosis of the squamous cell carcinoma subtype of non-small-cell lung cancer. Translational lung cancer Res. 2021;10(3):1221–30.
17. Amaravadi RK, Thompson CB. The roles of therapy-induced autophagy and necrosis in cancer treatment. Clin Cancer Res. 2007;13(24):7271–9.
18. White E, DiPaola RS. The double-edged sword of autophagy modulation in cancer. Clin Cancer Res. 2009;15(17):5308–16.
19. White E, Mehnert JM, Chan CS. Autophagy, metabolism, and Cancer. Clin Cancer Res. 2015;21(22):5037–46.
20. Chen P, Wu JN, Shu Y, Jiang HG, Zhao XH, Qian H, et al. Gemcitabine resistance mediated by ribonucleotide reductase M2 in lung squamous cell carcinoma is reversed by GW8510 through autophagy induction. Clin Sci. 2018;132(13):1417–33.
21. Zou Y, Xie J, Zheng S, Liu W, Tang Y, Tian W, et al. Leveraging diverse cell-death patterns to predict the prognosis and drug sensitivity of triple-negative breast cancer patients after surgery. Int J Surg. 2022;107:106936.
22. Ju M, Bi J, Wei Q, Jiang L, Guan Q, Zhang M et al. Pan-cancer analysis of NLRP3 inflammasome with potential implications in prognosis and immunotherapy in human cancer. Brief Bioinform. 2021;22(4).
23. Liu G, Xu X, Geng H, Li J, Zou S, Li X. FGA inhibits metastases and induces autophagic cell death in gastric cancer via inhibiting ITGA5 to regulate the FAK/ERK pathway. Tissue Cell. 2022;76:101767.
24. Wang M, Zhang G, Zhang Y, Cui X, Wang S, Gao S, et al. Fibrinogen alpha chain knockout promotes Tumor Growth and Metastasis through Integrin-AKT signaling pathway in Lung Cancer. Mol Cancer Res. 2020;18(7):943–54.
25. Wang C, Gu C, Jeong KJ, Zhang D, Guo W, Lu Y, et al. YAP/TAZ-Mediated upregulation of GAB2 leads to increased sensitivity to growth factor-Induced activation of the PI3K pathway. Cancer Res. 2017;77(7):1637–48.
26. Zhuo Y, Li S, Hu W, Zhang Y, Shi Y, Zhang F et al. Targeting SNORA38B attenuates tumorigenesis and sensitizes immune checkpoint blockade in non-small cell lung cancer by remodeling the tumor microenvironment via regulation of GAB2/AKT/mTOR signaling pathway. J Immunother Cancer. 2022;10(5).
27. Maki Y, Bos TJ, Davis C, Starbuck M, Vogt PK. Avian sarcoma virus 17 carries the Jun oncogene. Proc Natl Acad Sci U S A. 1987;84(9):2848–52.
28. Wang Y, Ran T, Li Y, Tian L, Yang L, Liu Z, et al. Identification of JUN gene and cellular microenvironment in response to PD-1 blockade treatment in lung cancer patients via single-cell RNA sequencing. Aging. 2024;16(12):10348–65.
29. Gutiontov SI, Turchan WT, Spurr LF, Rouhani SJ, Chervin CS, Steinhardt G, et al. CDKN2A loss-of-function predicts immunotherapy resistance in non-small cell lung cancer. Sci Rep. 2021;11(1):20059.
30. Galluzzi L, Vitale I, Aaronson SA, Abrams JM, Adam D, Agostinis P, et al. Molecular mechanisms of cell death: recommendations of the nomenclature Committee on Cell Death 2018. Cell Death Differ. 2018;25(3):486–541.
31. Kallunki T, Olsen OD, Jaattela M. Cancer-associated lysosomal changes: friends or foes? Oncogene. 2013;32(16):1995–2004.
32. Liang W, Liang H, Ou L, Chen B, Chen A, Li C, et al. Development and validation of a clinical risk score to predict the occurrence of critical illness in hospitalized patients with COVID-19. JAMA Intern Med. 2020;180(8):1081–9.

Publisher's note